Investigation on Radial Vibration of FSCW PMSM According to Pole/Slot Combination Considering Phase of Radial, Tangential Force and Moment

Jae-Hyun Kim, Jun-Yeol Ryu, Soo-Hwan Park, Kyoung-Soo Cha, Yun-Jae Won, *Graduate Student Member, IEEE*, Chi-Sung Park, and Myung-Seop Lim, *Senior Member, IEEE*

***Abstract*—In this study, the radial vibration of fractional-slot concentrated winding (FSCW) permanent magnet synchronous motor (PMSM) was analyzed according to pole/slot combination considering phase relationship of modulated radial, tangential forces, and moment. First, to calculate the modulated forces and moment according to pole/slot combination, the amplitude and phase of modulated radial, tangential force and moment converted by radial air-gap electromagnetic force density (AEFD) are analytically derived. Since the lever arm effect by tangential force varies according to the tooth length, tangential force was translated on the yoke and an equivalent modulated moment was derived. Subsequently, to analyze the radial vibration caused by modulated forces and moment, the radial displacement response owing to a unit radial AEFD is calculated using 3D structural finite element analysis by applying unit modulated forces and moment. It was found out that the tooth modulation effect hardly varied with pole/slot combination and shape of the PMSM such as tooth length. Rather, it was confirmed that the tooth modulation effect was significantly influenced by the slot opening width. Especially, it was analyzed that the radial vibration of PMSM is not simply reduced by optimizing the slot opening width with reduced modulated radial force, but the amplitude and phase of the modulated tangential force and moment should also be considered. Finally, four prototypes of the PMSM with different slot opening widths of two 12-slot 10-pole and two 12-slot 14-pole are fabricated, and the test and simulation results are compared and verified.**

***Index Terms*—Air-gap electromagnetic force density, fractional-slot concentrated winding permanent magnet synchronous motor, tooth modulation effect, vibration.**

Manuscript received 28 February 2023; revised 1 September 2023; accepted 10 October 2023. Date of publication 23 October 2023; date of current version 18 January 2024. Paper 2023-EMC-0220.R1, presented at the 2022 IEEE Energy Conversion Congress and Exposition, Detroit, MI, USA, Oct. 9–13, and approved for publication in the IEEE TRANSACTIONS ON INDUSTRY APPLICATIONS by the Electric Machines Committee of the IEEE Industry Applications Society [DOI: 10.1109/ECCE50734.2022.9947877]. This work was supported by the National Research Foundation of Korea funded by the Korea Government (MSIT) under Grant RS-2023-00207865. *(Corresponding author: Myung-Seop Lim.)*

Jae-Hyun Kim, Chi-Sung Park, and Myung-Seop Lim are with the Department of Automotive Engineering, Hanyang University, Seoul 04763, South Korea (e-mail: zerg1258@hanyang.ac.kr; chisung1226@hanyang.ac.kr; myungseop@hanyang.ac.kr).

Jun-Yeol Ryu is with Korea Automotive Technology Institute, Cheonan 31214, South Korea, and also with the Department of Automotive Engineering, Hanyang University, Seoul 04763, South Korea (e-mail: jyryu@katech.re.kr).

Soo-Hwan Park is with the Department of Mechanical, Robotics, and Energy Engineering, Dongguk University, Seoul 04620, South Korea (e-mail: parksh@dgu.ac.kr).

Kyoung-Soo Cha is with the Korea Institute of Industrial Technology, Daegu 42994, South Korea, and also with the Department of Automotive Engineering, Hanyang University, Seoul 04763, South Korea (e-mail: kscha@kitech.re.kr).

Yun-Jae Won is with the Department of Automotive Engineering (Automotive-Computer Convergence, Hanyang University, Seoul 04763, South Korea (e-mail: w961227@hanyang.ac.kr).

Color versions of one or more figures in this article are available at https://doi.org/10.1109/TIA.2023.3326425.

Digital Object Identifier 10.1109/TIA.2023.3326425

I. Introduction

FRACTIONAL-SLOT concentrated winding (FSCW) permanent magnet synchronous motors (PMSMs) are widely used in several industries owing to their high efficiency, high power density, low cogging torque, and excellent manufacturability [1]. However, FSCW PMSMs have a disadvantage of radial vibration characteristics because of their low spatial harmonic order of electromagnetic force caused by the armature magneto-motive force and stator slotting effect [2]. Accordingly, many studies have been conducted to improve the vibration characteristics of FSCW PMSMs while retaining the advantages [3], [4], [5], [6].

The radial vibration of the PMSM is inversely proportional to the fourth power of the spatial harmonic order of the air-gap electromagnetic force density (AEFD) [7]. Because the lowest spatial order of the AEFD is determined by the pole/slot combination, it is important to determine the pole/slot combinations at the initial design stage of FSCW PMSMs to maximize the lowest spatial harmonic order of the AEFD [8]. Recently, however, several studies have been actively conducted on high-order AEFDs that are modulated by the tooth-slot structure of the stator and act as low-order AEFDs [9], [10], [11], [12], [13], [14], [15], [16], [17], [18], [19]. Since this tooth modulation effect may be changed depending on the pole/slot combination, it is necessary to analyze it according to the pole/slot combination, not only considering the lowest spatial order of the AEFD.

Many studies have been conducted recently related to the tooth modulation effect. A previous study confirmed that vibration at $2f_e$ of the FSCW PMSM using bread-loaf PM was greater than that of the FSCW PMSM using conventional PM configuration [15]. In another study [16], an analytical model of the tooth modulation effect was derived, and it was discovered out that the slot opening width is an important factor that heavily influenced the tooth modulation effect. Mao et al. studied the vibration characteristics of the spoke-type machine with an asymmetric rotor considering the tooth modulation effect [17]. It

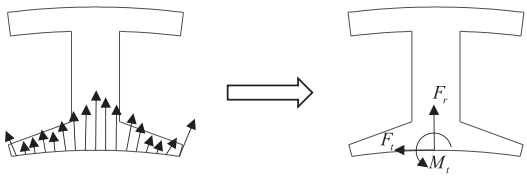

Fig. 1. Distributed AEFD and equivalent modulated force.

was discovered that an asymmetric rotor shape could effectively reduce torque ripple but degraded the vibration performance. In a previous study [18], unequal tooth design and PM flux density harmonics injection method were proposed to reduce vibrations caused by the modulated force. In [19], a hybrid model for vibration synthesis considering tangential force was proposed. However, in these studies, the modulation effect according to the pole/slot combination was not analyzed.

A few studies related to tooth modulation effect with respect to the pole/slot combination of the FSCW PMSM were also conducted recently. In [20], the difference in the force modulation effect of 12-slot 10-pole (12S10P) and 12-slot 14-pole (12S14P) PMSM were analyzed. However, although the force modulation effect was analyzed in detail, the analysis of the vibration characteristics in terms of the modulated force was insufficient. In addition, even though the slot opening width is important factor in tooth modulation effect, it was not investigated. In [21], research was conducted on the similarities and differences between the tooth modulation effect of the integer slot winding PMSM and FSCW PMSM. However, the modulation effect according to pole/slot combination was not considered. In [22], the force modulation effect with respect to the pole/slot combination of FSCW PMSMs was analyzed, and a vibration reduction design method was proposed by changing the slot opening width. However, only the radial modulated force by the radial AEFD was considered, and the modulated tangential force and moment were neglected. The radial AEFD generates not only a radial modulated force, but also a modulated tangential force and modulated moment, and these components are not negligible [19], [20].

This study analyzes the radial vibration of FSCW PMSM with respect to pole/slot combination considering phase relationship of modulated radial, tangential forces, and moment. Because the slot opening width influences the modulated forces and moment [15], the effect of the slot opening width on the tooth modulation effect is also investigated. In Section II, the force modulation effect was analytically derived and analyzed in detail in terms of the pole/slot combination and slot opening width. The amplitude and phase of the modulated radial and tangential forces, and moment caused by a unit radial AEFD were analytically derived. Here, since the displacement caused by tangential force is greatly affected by tooth length due to lever arm effect, the tangential force was translated on the yoke and an equivalent modulated moment was calculated. Subsequently, to analyze the radial vibration caused by modulated forces and moment, the radial displacement response due to the modulated forces and moment was calculated using 3D structural finite element analysis (FEA) in Section III. In Section IV, the vibration characteristics caused by the modulated forces and lowest order radial and tangential AEFD were analyzed and compared in terms of the slot opening width in the PMSM. Finally, to validate the modulation effect in the FSCW PMSM, the simulation and experimental results were compared.

II. Analysis of Radial Force Modulation Effect

A. Calculation Process of Radial Force Modulation Effect

In this section, the radial force modulation effect was analytically derived with respect to the pole/slot combination. Since the pole-number order tangential AEFD is relatively small compared to that of radial AEFD, only the modulation effect of radial AEFD is analyzed. It should be noted that this does not imply that the vibration caused by tangential AEFD can be ignored. Here, the slot opening width is also considered since it significantly affects the tooth modulation effect [15]. As shown in Fig. 1, the distributed radial and tangential AEFD can be equalized to the modulated radial and tangential forces, and moment. The modulated forces and moment can be expressed as the integration of the AEFD acting on the tooth tip, as expressed in (1)–(3) [20].

$$F_{r,z} = R_{si}L_{stk} \int_{\theta_z-\pi/S(1-\alpha)}^{\theta_z+\pi/S(1-\alpha)} \{f_r\cos(\theta_z-\theta)+f_t\sin(\theta_z-\theta)\}d\theta \quad (1)$$

$$F_{t,z} = R_{si}L_{stk} \int_{\theta_z-\pi/S(1-\alpha)}^{\theta_z+\pi/S(1-\alpha)} \{f_t\cos(\theta_z-\theta)-f_r\sin(\theta_z-\theta)\}d\theta \quad (2)$$

$$M_{t,z} = R_{si}^2L_{stk} \int_{\theta_z-\pi/S(1-\alpha)}^{\theta_z+\pi/S(1-\alpha)} f_r\sin(\theta_z-\theta)d\theta \quad (3)$$

Here, F and M_t are the modulated force and moment acting on the end of the tooth, respectively, f is the distributed AEFD, R_{si} is the inner radius of the stator, L_{stk} is the stack length, θ is the mechanical angle, θ_z is the mechanical angle of the center of the z^{th} tooth, α is the slot opening pitch, S is the number of slots, subscript r and t denote the radial and tangential directions, respectively, and z is the tooth number. Additionally, the moment term attributed to the tangential AEFD was ignored. The slot opening pitch indicates the ratio of the slot opening angle to the slot angle, and it can lie between 0 to 1. For instance, if the slot opening angle is 12° for 12 slots, the slot opening pitch is 0.4. As shown in (1)–(3), the radial AEFD generates a modulated radial force, tangential force, and moment. The modulated forces and moment caused by the nth spatial harmonic order radial AEFD are expressed as (4)–(6). Here, 1-α is expressed as β to simplify the equation.

$$F_{r,z} = f_{r,n}R_{si}L_{stk}\int_{\theta_z-\pi/S\beta}^{\theta_z+\pi/S\beta}\{\cos(n\theta)\cos(\theta_z-\theta)\}d\theta$$

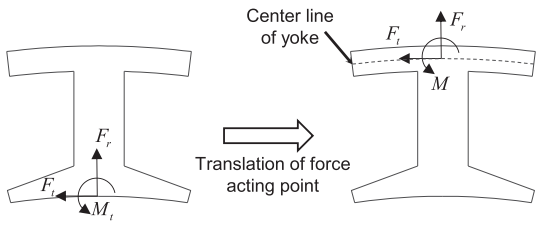

Fig. 2. Translation of force acting point to center of the yoke.

$$= f_{r,n} R_{si} L_{stk} \frac{2\cos(n\theta_z)\left\{n\cos\left(\frac{\pi\beta}{S}\right)\sin\left(\frac{n\pi\beta}{S}\right) - \sin\left(\frac{\pi\beta}{S}\right)\cos\left(\frac{n\pi\beta}{S}\right)\right\}}{n^2-1} \tag{4}$$

$$F_{t,z} = -f_{r,n} R_{si} L_{stk} \int_{\theta_z-\pi/S\beta}^{\theta_z+\pi/S\beta} \{\cos(n\theta)\sin(\theta_z-\theta)\}d\theta$$
$$= -f_{r,n} R_{si} L_{stk} \frac{2\sin(n\theta_z)\left\{\cos\left(\frac{\pi\beta}{S}\right)\sin\left(\frac{n\pi\beta}{S}\right) - n\sin\left(\frac{\pi\beta}{S}\right)\cos\left(\frac{n\pi\beta}{S}\right)\right\}}{n^2-1} \tag{5}$$

$$M_{t,z} = f_{r,n} R_{si}^2 L_{stk} \int_{\theta_z-\pi/S\beta}^{\theta_z+\pi/S\beta} \{\cos(n\theta)\sin(\theta_z-\theta)\}d\theta$$
$$= f_{r,n} R_{si}^2 L_{stk} \frac{2\sin(n\theta_z)\left\{\cos\left(\frac{\pi\beta}{S}\right)\sin\left(\frac{n\pi\beta}{S}\right) - n\sin\left(\frac{\pi\beta}{S}\right)\cos\left(\frac{n\pi\beta}{S}\right)\right\}}{n^2-1} \tag{6}$$

As shown in (4)–(6), the contribution of the radial AEFD to the modulated force is affected by the spatial harmonic order of the radial AEFD n, number of slots S, and slot opening pitch α ($= 1 - \beta$). However, if the point where the tangential force is applied is located at the end of the tooth as shown in Fig. 1, the radial displacement or vibration caused by the tangential force changes according to the length of the tooth, thus it is difficult to calculate the tooth modulation effect in general. The displacement due to the modulated radial force and moment is independent of the position where the force acts, but as the tangential force creates a lever arm effect, the displacement varies depending on the force acting point. Therefore, to exclude the influence of the displacement response by the tangential force with respect to the tooth length, the force acting point was moved to the center of the yoke as shown in Fig. 2. Accordingly, the modulated moment acting on the center of the yoke can be expressed as follows:

$$M_z = M_{t,z} - F_{t,z}\left(R_{so} - R_{si} - \frac{t_{yoke}}{2}\right)$$
$$\approx f_{r,n} R_{si} R_{so} L_{stk} \frac{2\sin(n\theta_z)\left\{\cos\left(\frac{n\pi}{S}\right)\sin\left(\frac{n\pi\beta}{S}\right) - n\sin\left(\frac{\pi\beta}{S}\right)\cos\left(\frac{n\pi\beta}{S}\right)\right\}}{n^2-1} \tag{7}$$

TABLE I
MAJOR PARAMETERS OF THE TARGET PMSMS

Item	Value	Unit
Stator outer radius	100.0	mm
Stator inner radius	50.0	mm
Stack length	50.0	mm
Slot opening pitch	0 – 0.8	-

where M is the modulated moment, R_{so} is the stator outer radius, and t_{yoke} is the yoke thickness. In general, because the stator outer radius is significantly larger than the yoke thickness, the yoke thickness term is ignored for simplicity. The total modulated moment is proportional to the stator outer radius, unlike other modulated forces.

B. Force Modulation Effect According to Pole/Slot Combination and Slot Opening Pitch

The amplitudes of the modulated forces and moment were calculated according to the spatial order of the AEFD, number of slots, and slot opening pitch based on (4)–(7). It should be mentioned that since it is impossible to represent all pole/slot combinations, only the pole/slot combinations where the number of the slot is below 30 and $2p = S \pm 2$ are analyzed in this study, where p is the pole pair. Therefore, the pole/slot combinations of 6S4P, 6S8P, 12S10P, 12S14P, 18S16P, 18S20P, 24S22P, and 24S26P were analyzed. It does not imply that the analysis is applicable only to these pole/slot combinations, and the modulated forces and moment for other pole/slot combinations can still be calculated using (4)–(7). To calculate the modulated forces and moment caused by a unit radial AEFD, the outer and inner radii of the stator core are required. The major parameters of the stator to be analyzed are listed in Table I. The modulated forces by the unit radial AEFD were calculated according to the force order, number of slots, and slot opening pitch, and the results are shown in Fig. 3. Here, since the modulated force is the largest at twice the fundamental frequency [20], $2f_e$, only the pole number spatial order radial AEFD is considered. It is noteworthy that this does not imply that the tooth modulation effect does not occur in other time harmonic order. However, if the waveform of the magneto-motive force by the PM is designed sinusoidally, the electromagnetic force of the high time harmonic order can be minimized. Therefore, in this study, we focused on $2f_e$ caused by the synthesis of the fundamental magneto-motive force. It should be noted that the modulated moment is not shown as the amplitude trend of the modulated moment is the same to that of the modulated tangential force. Although the exact amplitudes are different according to the pole/slot combination, the amplitude trend of the pole/slot combinations with $2p = S - 2$ are similar, and that of $2p = S + 2$ are also similar. For $2p = S - 2$, the modulated radial force increases and then decreases as the slot opening pitch increases, while the tangential force and moment decrease monotonically. For $2p = S + 2$, there exists a slot opening pitch at which the modulated radial force becomes zero. The tangential force and moment increase and then decrease as the slot opening pitch increases. At the slot opening pitch $\alpha = \alpha_{\min}$, where the modulated radial force

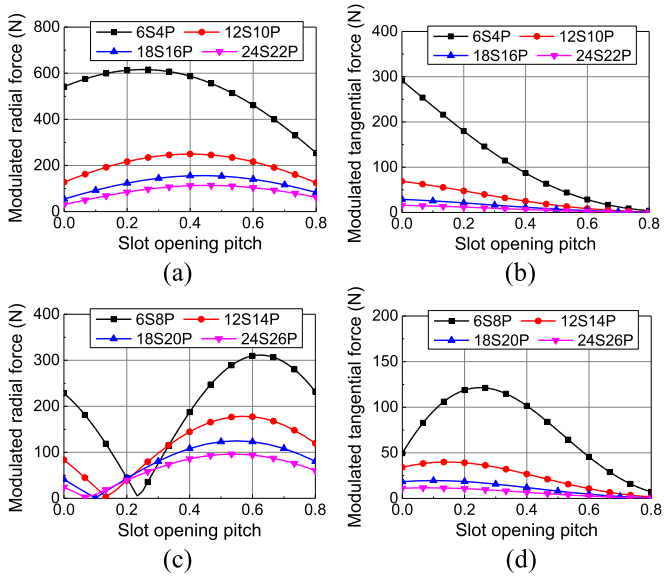

Fig. 3. Amplitude of modulated forces by unit radial AEFD according to the slot opening pitch. (a) $2p = S - 2$ radial force. (b) $2p = S - 2$ tangential force. (c) $2p = S + 2$ radial force. (d) $2p = S + 2$ tangential force.

becomes zero, the radial vibration cannot be guaranteed to be minimized because the tangential force and moment are maximized. The displacement or vibration cannot be determined only from the amplitudes of the modulated forces and moment. It is necessary to determine the displacement response caused by the unit modulated forces and moment, and the phase relationship of the forces to calculate the displacement at which these modulated forces act simultaneously.

Therefore, the amplitude and phase relationship between the modulated forces and moment are analyzed in this section, and the displacement caused to the unit modulated force and moment is discussed in the next section. For $2p = S \pm 2$, the main spatial harmonic order n of the radial AEFD at twice the fundamental frequency, $2f_e$, is $S \pm 2$. By substituting the above (4), (5), and (7), the modulated forces and moment are expressed as follows:

$$F_{r,z} = f_{r,n} R_{si} L_{stk} K_r(\alpha) \cos\left\{(S \pm 2)\frac{2\pi}{S} z\right\} = f_{r,n} R_{si} L_{stk} K_r(\alpha) \cos\left(\frac{4\pi}{S} z\right) \tag{8}$$

$$F_{t,z} = -f_{r,n} R_{si} L_{stk} K_t(\alpha) \sin\left\{(S \pm 2)\frac{2\pi}{S} z\right\} = f_{r,n} R_{si} L_{stk} K_t(\alpha) \cos\left(\frac{4\pi}{S} z \pm \frac{\pi}{2}\right) \tag{9}$$

$$M_z = f_{r,n} R_{si} R_{so} L_{stk} K_t(\alpha) \sin\left\{(S \pm 2)\frac{2\pi}{S} z\right\} = f_{r,n} R_{si} R_{so} L_{stk} K_t(\alpha) \cos\left(\frac{4\pi}{S} z \mp \frac{\pi}{2}\right) \tag{10}$$

TABLE II
PHASE OF MODULATED FORCE AND DISPLACEMENT WHEN $2P = S - 2$

Force order	Modulated force	Phase of force	Phase of radial displacement
$2p = S - 2$	Radial	0°	0°
	Tangential	–90°	180°
	Moment	90°	180°

TABLE III
PHASE OF MODULATED FORCE AND DISPLACEMENT WHEN $2P = S + 2$

Force order	Slot opening pitch	Modulated force	Phase of force	Phase of radial displacement
$2p = S + 2$	$\alpha > \alpha_{\min}$	Radial	180°	180°
	$\alpha < \alpha_{\min}$	Radial	0°	0°
		Tangential	90°	0°
		Moment	-90°	0°

where,

$$K_r(\alpha) = \frac{2\left\{n\cos\left(\frac{\pi\beta}{S}\right)\sin\left(\frac{n\pi\beta}{S}\right) - \sin\left(\frac{\pi\beta}{S}\right)\cos\left(\frac{n\pi\beta}{S}\right)\right\}}{n^2 - 1} \tag{11}$$

$$K_t(\alpha) = \frac{2\left\{\cos\left(\frac{\pi\beta}{S}\right)\sin\left(\frac{n\pi\beta}{S}\right) - n\sin\left(\frac{\pi\beta}{S}\right)\cos\left(\frac{n\pi\beta}{S}\right)\right\}}{n^2 - 1} \tag{12}$$

Therefore, for $2p = S - 2$, the phase of the modulated radial force leads the tangential force by 90° and lags the moment by 90°. Since the phase of the radial displacement caused by the tangential force lags by 90° from that caused by the radial force [19], the phases of the radial displacement by radial force and radial displacement by tangential force differ from each other by 180°. This indicates that the radial displacement or vibration caused by the modulated radial force and tangential force suppress each other. Similarly, since the phase of the radial displacement caused by the modulated moment leads that of the displacement caused by the radial force by 90° [19], the displacement caused by the moment and radial force also differ from each other by 180° and suppress each other. The phase relationship between the modulated forces and displacement when $2p = S - 2$ is summarized in Table II.

For the case of $2p = S + 2$, different from $2p = S - 2$, the phase of the modulated radial force lags the phase of the tangential force by 90° and leads the phase of the moment by 90°. This indicates that the radial displacement due to the modulated radial and tangential forces and moment enhance each other. The phase relationship between the modulated forces and displacement in terms of the slot opening pitch when $2p = S + 2$ is summarized in Table III. The amplitude and phase relationships of the modulated radial and tangential forces, and moment with respect to the force order, number of slots, and slot opening pitch were calculated, but the amplitude of the radial displacement was not investigated. The displacement response caused by the modulated forces and moment is analyzed in the next section.

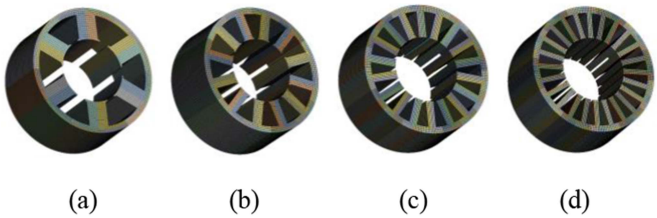

Fig. 4. Configuration of the 3D structural model. (a) 6 slots. (b) 12 slots. (c) 18 slots. (d) 24 slots.

TABLE IV
MAJOR PARAMETERS OF THE STRUCTURAL MODEL

Item	Value	Unit
Core material	50PN470	-
Yoke thickness	5.0	mm
Young's modulus	180	GPa
Shear modulus	69.2	GPa
Poisson's ratio	0.3	-
Density	7700	kg/m^3

III. DISPLACEMENT RESPONSE BY UNIT RADIAL AEFD

In this section, to analyze the tooth modulation effect, the radial displacement response is calculated for each spatial harmonic order of the radial AEFD, number of slots, and slot opening pitch. Even though torque ripple also can deteriorate the vibration of PMSM, the dominant vibration of PMSM is generally caused by radial force of PMSM [17]. Therefore, in this study, the torque ripple was not investigated. To apply the distributed unit radial AEFD to the structural model, the structural models for each slot opening pitch should be developed. However, because the slot opening pitch does not affect the stiffness of the motor, the radial displacement response caused by the unit concentrated force was calculated instead of the distributed AEFD to reduce the computation time. Subsequently, by multiplying the radial displacement response caused by the unit concentrated forces of 2nd spatial order and calculated modulated forces based on (8)–(12), the total radial displacement response caused by the unit radial AEFD was calculated as follows:

$$Y = F_r e^{j\psi_{Fr}} y_r e^{j0} + F_t e^{j\psi_{Ft}} y_t e^{\frac{-j\pi}{2}} + M e^{j\psi_M} y_M e^{\frac{j\pi}{2}} \quad (13)$$

where Y is the total displacement response, y is the displacement response caused by the unit modulated force, and ψ is the electrical phase angle of the modulated force.

A. Displacement Response by Unit Modulated Forces

To calculate the radial displacement caused by the unit radial AEFD using (13), the displacement caused by the unit concentrated force was calculated. The radial displacement response was calculated by 3D structural FEA using the commercial software ANSYS. The 3D structural model was built by modeling only the stator core as shown in Fig. 4, neglecting the enclosure and winding. The major parameters of the structural model are listed in Table IV. To apply the 2nd spatial order force to the structural model, the phase difference of the force for each tooth was set to π / S. For instance, to apply 2nd order force to 12 slots, the phase difference for each tooth was set to 60° as shown in Fig. 5. To neglect the effect of resonance, the frequency of force was set to 10 Hz.

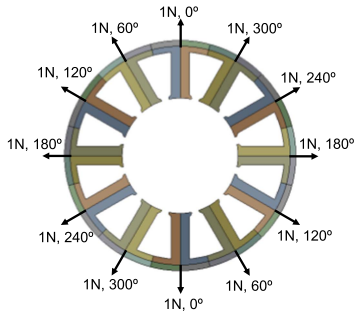

Fig. 5. 2nd order concentrated force application to structural model.

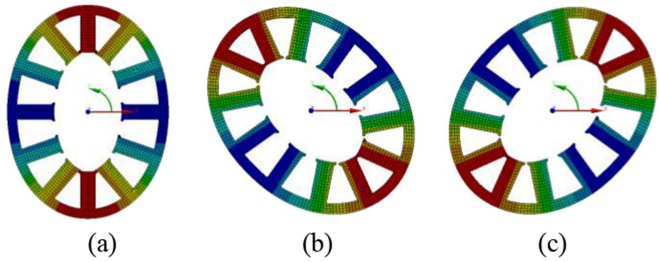

Fig. 6. Displacement response of 12-slot structure by unit 2nd spatial order concentrated force. (a) Radial force. (b) Tangential force. (c) Moment.

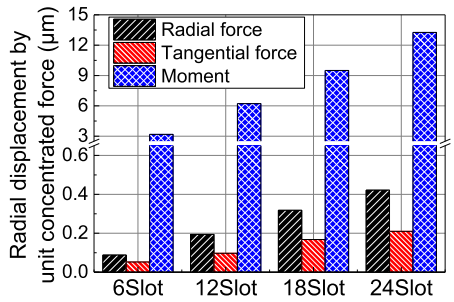

Fig. 7. Radial displacement response by unit modulated force.

Fig. 6 shows the displacement response when unit modulated forces and moment of the 2nd order are applied to the 12-slot structural model. As mentioned earlier, the radial force and displacement have the same phase and radial displacement lag/lead the tangential force/moment 90°. The radial displacement has a 2nd mode shape, and the maximum displacements for each slot number are shown in Fig. 7. Although the radial displacement response with respect to the unit force varies with the number of slots, the ratio of the amplitude of the radial displacement by the radial and tangential forces and moment does not change significantly.

B. Tooth Modulation Effect by Unit Radial AEFD

The radial displacement responses caused by the unit AEFD were calculated with respect to the spatial order of AEFD,

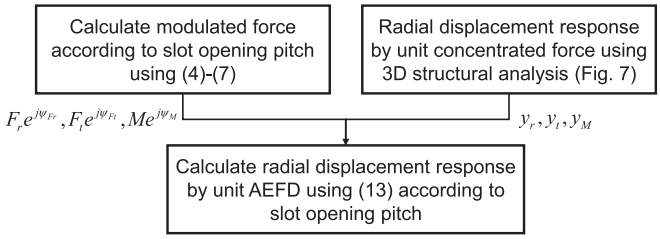

Fig. 8. Calculation process of displacement response caused by unit AEFD with respect to slot opening pitch.

number of slots, and slot opening pitch by substituting the amplitude and phase of the concentrated force caused by the unit AEFD (calculated in Section II) and the radial displacement response caused by the unit concentrated force into (13). Fig. 8 shows the calculation process of the radial displacement response by the unit AEFD. Even if the process of transforming distributed forces into equivalent concentrated forces is correct, the local displacement caused by the two forces may be different. However, according to Saint-Venant's principle, if the location of the point where the displacement is obtained is sufficiently far from the point where the force acts, the displacement caused by the distributed force and equivalent concentrated forces are the same [23]. In this study, the force is acting on the tooth tip and the displacement is obtained from the outer surface of the stator, so this displacement calculation process is reasonable.

The calculated radial displacement with respect to the slot opening pitch caused by the unit AEFD is shown in Fig. 9. Based on the conventional displacement equation assuming the shape of the stator as a cylinder model, the radial displacement is inversely proportional to the fourth power of the spatial harmonic order of AEFD as follows:

$$Y(\nu \geq 2) = \frac{12 R_{si} R_{yoke}^3}{E t_{yoke}^3 (r^2 - 1)^2} f_r, \ (|r| = \nu) \qquad (14)$$

where R_{yoke} is the average yoke radius, ν is the vibration mode number, r is the spatial harmonic order of AEFD, and E is the elastic modulus of the equivalent ring model. Therefore, when the slot opening pitch is 0, the smaller the force order, the larger is the radial displacement. However, when the slot opening pitch exceeds 0, the displacement caused by the high-order AEFD is larger owing to the tooth modulation effect. Especially, the radial displacement is maximum when the slot opening pitch is 0.5, regardless of the number of pole/slot combinations. Although the modulated radial force in the condition $2p = S + 2$ is minimized at the slot opening pitch $\alpha = \alpha_{\min}$, the displacement is not minimized. Therefore, it is confirmed that the modulated tangential force and moment should be considered for analyzing the tooth modulation effect owing to the high-order radial AEFD. These results are almost constant regardless of the size or shape of the motor. In (7), the tangential force was converted into moment to ignore the difference in displacement with respect to the tooth length owing to the tangential force. The modulated moment itself differs from the modulated radial and tangential forces in that it is proportional to the stator outer radius. However,

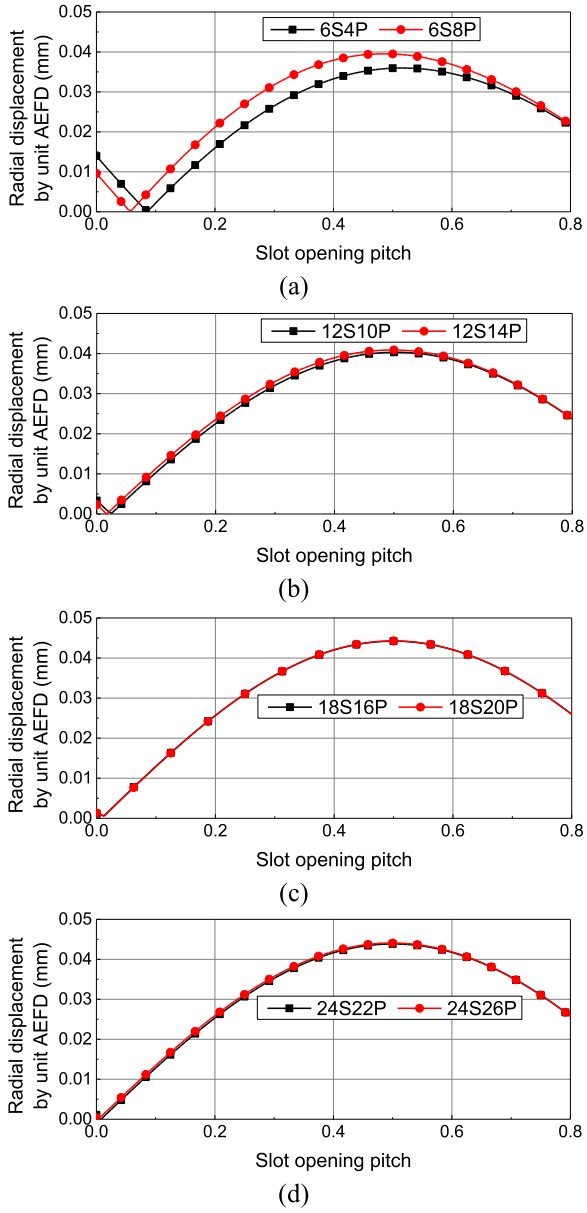

Fig. 9. Radial displacement caused by unit AEFD according to slot opening pitch. (a) 6 slots. (b) 12 slots. (c) 18 slots. (d) 24 slots.

the displacement by moment is proportional to $R^2{}_{yoke}$ [24], and displacement by radial and tangential force is proportional to $R^3{}_{yoke}$. Therefore, even if the configuration of the motor changes, the displacement trend does not change. As shown in the results, in the pole/slot combination with $2p = S \pm 2$, the slot opening pitch from 0.5 should be avoided to minimize the tooth modulation effect.

IV. Verification of Tooth Modulation Effect on PMSM Vibration

In this section, the tooth modulation effect on the PMSM vibration characteristics was verified through 3D vibration FEA and tests of the $2p = S \pm 2$ PMSMs. As shown in Fig. 9, the

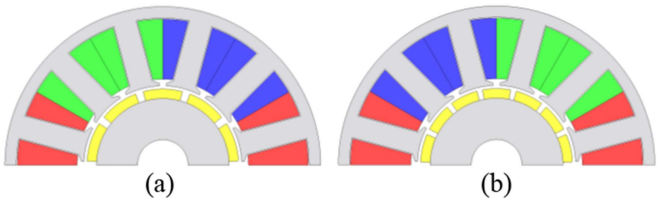

Fig. 10. Configuration of the $2p = S \pm 2$ PMSMs. (a) 12S10P. (b) 12S14P.

TABLE V
SPECIFICATIONS OF 12S10P AND 12S14P PMSMS

Item	Unit	Value
		12S10P & 12S14P
Stator outer diameter	mm	100.0
Rotor outer diameter	mm	48.0
Stack length	mm	50.0
Tooth width	mm	7.3
Yoke width	mm	3.65
Air-gap length	mm	1.0
PM height	mm	3.0
Pole arc/pole pitch ratio	-	0.8
PM remanence	T	1.2
Slot opening pitch	-	0.1 - 0.4
Rated torque	Nm	5.0
Rated rotational speed	rpm	1000

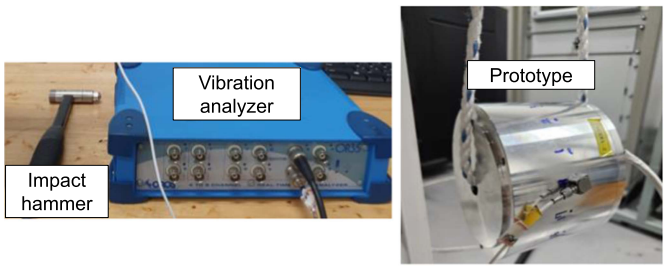

Fig. 11. Modal test setup.

difference in the modulation effect was not significant regardless of the pole/slot combination, thus, verification was conducted on the 12S10P PMSM with $2p = S - 2$ and 12S14P PMSM with $2p = S + 2$.

A. Modal Analysis

In order to compare the vibration test and vibration analysis results, modeling of the motor enclosure is required. To confirm the reliability of the vibration analysis results, the modal test results were compared to the modal simulation results. The stator structure of the PMSM is complicated due to the laminated stator core and winding. Therefore, the equivalent material properties were obtained through parametric fitting [20]. The configuration and specifications of the models are shown in Fig. 10 and Table V. Fig. 11 shows the modal test setup of 12S10P PMSM with slot opening pitch of 0.166. Through the modal test, the natural frequencies, modal shapes, and damping ratios were obtained. Then, the equivalent material parameters were obtained using the modal test results and modal simulation results using ANSYS, and it is summarized in Table VI. Since the spatial

TABLE VI
EQUIVALENT MATERIAL PROPERTIES

Items		Stator core	Winding	Enclosure
Density (kg/m^3)	-	7700	8930	2700
Young's modulus (GPa)	E_x	180		
	E_y	180	1	68.9
	E_z	109.5		
Poisson's ratio	u_{xy}	0.3		
	u_{yz}	0.15	0.1	0.33
	u_{xz}	0.15		
Shear modulus (GPa)	G_{xy}	38.3		
	G_{yz}	4.5	0.4	25.9
	G_{xz}	4.5		

TABLE VII
MODAL TEST AND SIMULATION RESULTS

Simulated	Measured	Relative error	Damping ratio
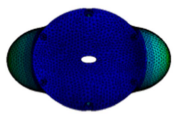	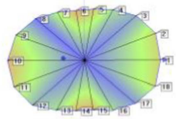	3.65%	0.83%
3348 Hz	3230 Hz		

order of the main electromagnetic force of the 12S10P PMSM is 2 mode, the results of the 2 mode shape are summarized in Table VII. The relative error between measured and simulated result is 3.65%, which is agreeable.

B. Vibration Caused by Modulation Effect of $2p = S \pm 2$ PMSMs

For 12S10P/12S14P PMSMs with the pole/slot combinations of $2p = S \pm 2$, the vibration characteristics owing to the modulation effect were analyzed through 3D vibration FEA using the commercial software ANSYS. The maximum slot opening pitch was determined by considering the tooth width. In general, as the load increases, the vibration caused by the lowest-order AEFD dominates over the high-order AEFD [18]. Therefore, the vibration was analyzed with respect to the slot opening pitch in the no-load and rated load condition. The radial and tangential AEFDs were calculated with respect to the slot opening pitch using 2D electromagnetic FEA based on the Maxwell stress tensor method, and the displacement response caused by the AEFD was obtained for each spatial order using 3D structural FEA based on (13). Fig. 12 shows the amplitude trend of the lowest and pole-number order radial AEFD with respect to the slot opening pitch. Depending on the amplitude of the load, the amplitude of the pole-number order radial AEFD caused by the synthesis of fundamental component did not change significantly, while the amplitude of the lowest-order radial AEFD increased as the load increased. As the slot opening pitch increases, the magnetic field itself changes because the saturation and relative permeance change. The fundamental component of the magnetic field decreases, and the harmonic components increase. Therefore, the lowest-order AEFD increases and the pole-number order AEFD decreases. However, although the amplitude of the pole-number order AEFD decreases, it can be predicted that the vibration

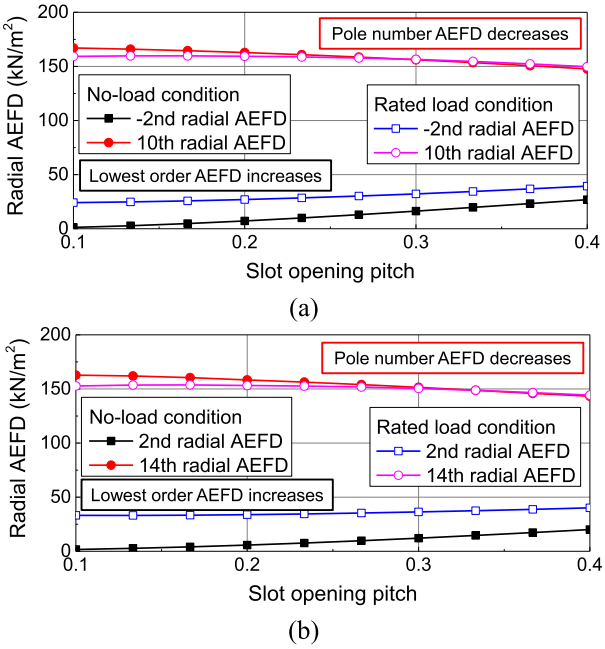

Fig. 12. Radial AEFD amplitude of the lowest and pole number order according to slot opening pitch at no-load and rated load condition. (a) 12S10P. (b) 12S14P.

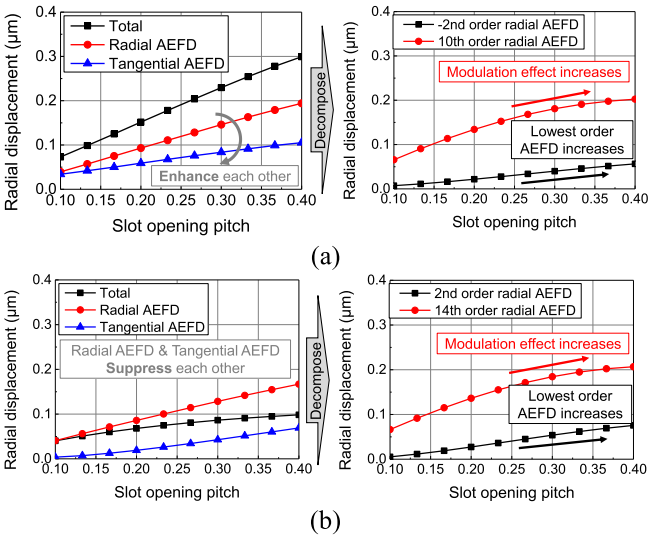

Fig. 13. Radial displacement according to slot opening pitch at no-load condition. (a) 12S10P. (b) 12S14P.

increases as the slot opening pitch increases because the modulation effect increases as shown in Fig. 9, regardless of the load condition. Figs. 13 and 14 show the radial displacement of the 12S10P and 12S14P PMSMs with respect to the slot opening pitch at no-load condition and rated load condition, respectively. Regardless of the load condition, for the 12S10P PMSM with $2p = S - 2$, the radial displacement by radial AEFD and tangential AEFD are in the same phase, thus, the displacement is large. For the 12S14P PMSM with $2p = S + 2$, regardless of the load condition, the radial displacement by the radial AEFD

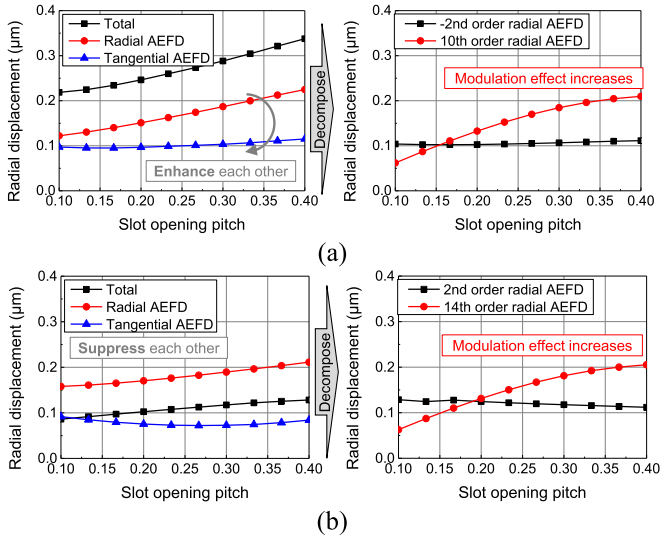

Fig. 14. Radial displacement according to slot opening pitch at rated load condition. (a) 12S10P. (b) 12S14P.

and tangential AEFD are in opposite phases, which leads a small radial displacement.

To investigate the influence of the modulation effect on PMSM vibration, the radial displacement caused by the radial AEFD is decomposed by spatial order and shown on the right side of Figs. 13 and 14. At no-load condition, common to both the 12S10P and 12S14P PMSM, the radial displacement by the pole-number order radial AEFD is dominant, which is induced by the tooth modulation effect. However, under the rated load condition, it can be seen that the radial displacement caused by the lowest-order radial AEFD is as large as the pole-number order radial AEFD. In other words, it can be confirmed that the radial vibration caused by the tooth modulation effect becomes dominant as the load decreases. Regardless of the load condition, the displacements of the PMSMs caused by 10^{th} order and 14^{th} order radial AEFD show approximately similar amplitudes, which implies that there is almost no difference in the tooth modulation effect caused by the two AEFDs, as analyzed in Section III. As explained above, even the amplitude of the pole-number order radial AEFD decreases as the slot opening pitch increases because magnetic field changes itself when slot opening pitch varies, the radial displacement increases as the tooth modulation effect increases.

C. Experimental Verifications

To verify the tooth modulation effect with respect to the slot opening pitch, vibration tests were conducted on the prototypes of 12S10P and 12S14P PMSMs with different slot opening pitches. Four prototypes with two 12S10P PMSMs and two 12S14P PMSMs were fabricated with slot opening pitches of 0.166 and 0.4, respectively. For convenience, the 12S10P PMSM models with slot opening pitch 0.166 and 0.4 are named Model A and Model B, respectively, and the 12S14P PMSM models with slot opening pitch of 0.166 and 0.4 are named Model C and Model D, respectively; the details are summarized in Table VIII.

TABLE VIII
INFORMATION ON THE FOUR PROTOTYPES

Model name	Pole/slot combination	Slot opening pitch
Model A	12S10P	0.166
Model B	12S10P	0.4
Model C	12S14P	0.166
Model D	12S14P	0.4

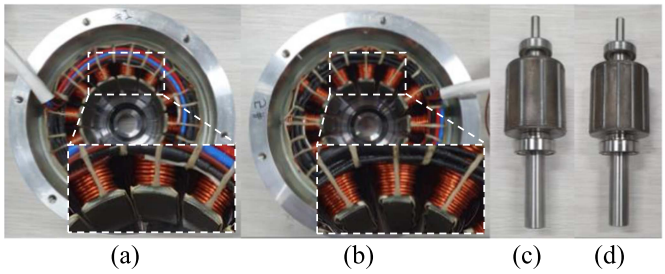

Fig. 15. Prototypes of 12S10P and 12S14P PMSMs with different slot opening pitch. (a) Slot opening pitch 0.166 stator. (b) Slot opening pitch 0.4 stator. (c) 12S10P rotor. (d) 12S14P rotor.

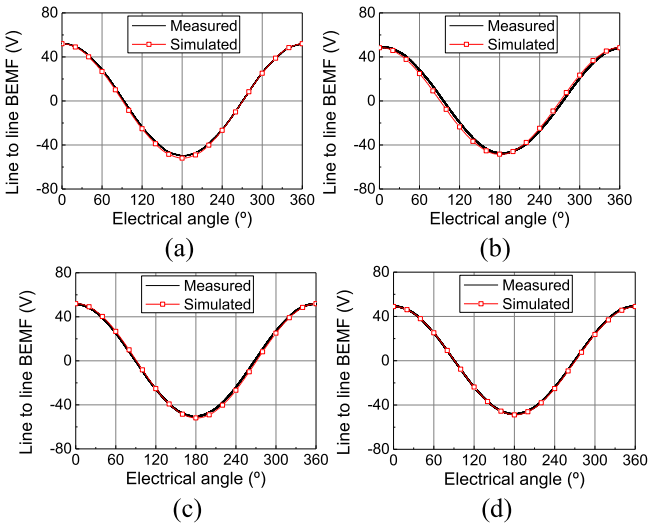

Fig. 16. Measured and simulated back electro-motive force at 1000 rpm. (a) Model A. (b) Model B. (c) Model C. (d) Model D.

Fig. 15 shows the shapes of the stator with different slot opening pitches, and rotors of the prototypes. To validate whether the prototypes were fabricated correctly, the back electro-motive force (BEMF) was measured and compared with the 2D electromagnetic FEA results at 1000 rpm. Fig. 16 shows the measured and simulated BEMF results, and it was confirmed that the tests and FEA results were in good agreement.

Fig. 17 shows the vibration test setup, which includes a prototype, load motor, accelerometer, data acquisition, and vibration analyzer. The vibration test at no-load condition and rated load condition was performed by rotating the prototype at 1000 rpm by the load motor, and four accelerometers were attached to the surface of the prototype enclosure, two at the center of the slot and two at the center of the tooth. The measured time domain accelerations were converted into frequency domain,

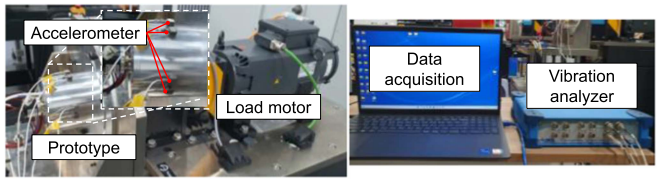

Fig. 17. Vibration test setup.

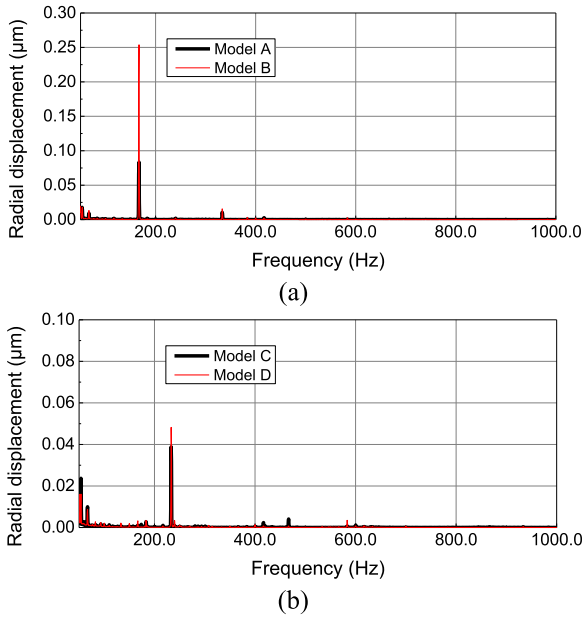

Fig. 18. Vibration test results of four prototypes at no-load condition at 1000 rpm. (a) 12S10P. (b) 12S14P.

and the average acceleration was calculated. Subsequently, the square of each angular frequency was divided by the acceleration to calculate the radial displacement. The measured radial displacements at no-load condition and rated load condition are shown in Figs. 18 and 19, respectively. For the 12S10P PMSM at no-load condition, the vibration of Model B with a larger slot opening pitch is significantly larger than Model A with a smaller slot opening pitch. This is mainly caused by an increased tooth modulation effect, and an increased amplitude of the lowest-order radial and tangential AEFD, as depicted in Fig. 13. At rated load condition, still the vibration of Model B is larger than Model A. However, it can be seen that the radial vibration difference between the two models is reduced compared to the no-load condition. This was due to an overall increase in vibration due to an increase in the lowest-order radial AEFD as the load increased. It can be seen that as the load increases, the difference in vibration between models due to the tooth modulation effect decreases. However, it still implies that the for pole/slot combination with $2p = S - 2$ PMSM, a smaller slot opening pitch can reduce vibrations.

For the 12S14P PMSM, similar results were obtained. At no-load and rated load conditions, the vibration of Model D with a larger slot opening pitch is larger than Model C with a smaller slot opening pitch, as expected. However, the vibration of the

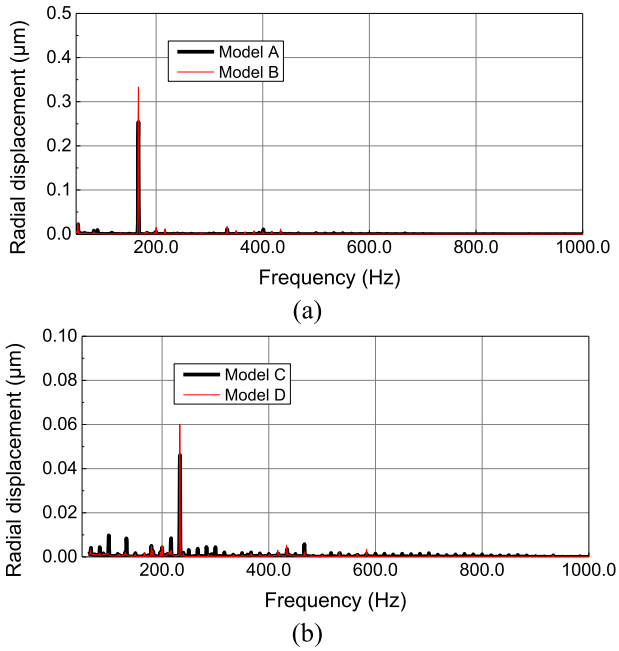

Fig. 19. Vibration test results of four prototypes at rated load condition at 1000 rpm. (a) 12S10P. (b) 12S14P.

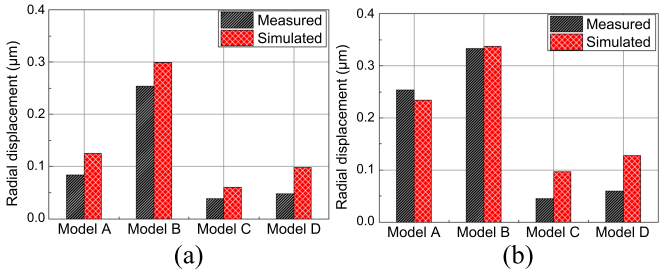

Fig. 20. Vibration test and FEA results at $2f_e$. (a) No-load condition. (b) Rated load condition.

12S14P PMSM was smaller than that of the 12S10P PMSM, and the increased vibration ratio with respect to the slot opening pitch was also smaller than that of the 12S10P PMSM. This is because the tangential AEFD increases simultaneously with the modulation effect as the slot opening increases, and the displacements caused by the radial and tangential AEFD suppress each other, as described previously. Fig. 20 shows the measured and simulated radial displacement results at no-load condition and rated load condition of the four prototypes. Although the two results are not completely identical, it can be confirmed that the radial displacement increases as the slot opening pitch increases, and that the radial displacement of the $2p = S - 2$ PMSM is greater than that of the $2p = S + 2$ PMSM.

V. Conclusion

In this study, the tooth modulation effect was investigated in terms of the pole/slot combination and slot opening pitch. First, the force modulation effect caused by the unit radial AEFD was analytically derived. Here, the tangential force was translated into the center of the yoke to neglect the lever arm effect and an equivalent moment was calculated for a compensation. It was found out that for $2p = S - 2$, the amplitude of modulated radial, tangential force and moment is greater than $2p = S + 2$. However, considering the phase relationship between modulated forces and moment, it cannot be concluded that the radial vibration of $2p = S - 2$ will be greater. Therefore, to analyze the tooth modulation effect, 3D structural FEA was performed by applying modulated forces. Unlike the force modulation effect, the radial displacement by the modulated radial and tangential forces and moment is enhanced/suppressed, confirming that there is no significant difference in the tooth modulation effect with respect to the pole/slot combination and shape of the motor such as tooth length. Rather, it was confirmed that the tooth modulation effect is greatly affected by the slot opening pitch. Then, the radial and tangential AEFDs for each spatial harmonic order were calculated with respect to the slot opening pitch of the 12S10P and 12S14P PMSMs, and the vibration caused by each harmonic order AEFD was calculated. The modulation effect increased as the slot opening pitch increased, and the effect of the lowest spatial order radial and tangential AEFD also increased. However, for $2p = S \pm 2$, the radial and tangential AEFD vibrations were suppressed and enhanced, respectively, so the total radial displacement response was smaller in $2p = S + 2$ than in $2p = S - 2$. Finally, two prototypes of 12S10P PMSMs and two of 12S14P PMSMs were manufactured, and results were verified through experiments.

References

[1] J.-H. Kim, J.-Y. Ryu, S.-H. Park, K.-S. Cha, C.-S. Park, and M.-S. Lim, "Tooth modulation effect of electromagnetic force on fractional slot concentrated winding PMSM according to slot opening," in *Proc. IEEE Energy Convers. Congr. Expo.*, 2022, pp. 1–5.

[2] T. Sun, J.-M. Kim, G.-H. Lee, J.-P. Hong, and M.-R. Choi, "Effect of pole and slot combination on noise and vibration in permanent magnet synchronous motor," *IEEE Trans. Magn.*, vol. 47, no. 5, pp. 1038–1041, May 2011.

[3] Z. Wu, Y. Fan, H. Wen, and D. Gao, "Vibration suppression of FSCW-IPM with auxiliary slots," in *Proc. IEEE Energy Convers. Congr. Expo.*, 2018, pp. 3222–3227.

[4] F. Lin, S. G. Zuo, W. Z. Deng, and S. L. Wu, "Reduction of vibration and acoustic noise in permanent magnet synchronous motor by optimizing magnetic forces," *J. Sound Vib.*, vol. 429, pp. 193–205, 2018.

[5] S. Zuo, F. Lin, and X. Wu, "Noise analysis, calculation, and reduction of external rotor permanent-magnet synchronous motor," *IEEE Trans. Ind. Electron.*, vol. 62, no. 10, pp. 6204–6212, Oct. 2015.

[6] P. Asef, R. B. Perpina, and A. C. Lapthorn, "Optimal pole number for magnetic noise reduction in variable-speed permanent magnet synchronous machines with fractional-slot concentrated windings," *IEEE Trans. Transp. Electrific.*, vol. 5, no. 1, pp. 126–134, Mar. 2019.

[7] S. J. Yang, *Low-Noise Electrical Motors*. Oxford, U.K.: Clarendon, 1981.

[8] D.-Y. Kim, M.-R. Park, J.-H. Sim, and J.-P. Hong, "Advanced method of selecting number of poles and slots for low-frequency vibration reduction of traction motor for elevator," *IEEE/ASME Trans. Mechatron.*, vol. 22, no. 4, pp. 1554–1562, Aug. 2017.

[9] H. Fang, D. Li, R. Qu, and P. Yan, "Modulation effect of slotted structure on vibration response in electrical machines," *IEEE Trans. Ind. Electron.*, vol. 66, no. 4, pp. 2998–3007, Apr. 2019.

[10] R. Pile, Y. L. Menach, J. L. Besnerais, and G. Parent, "Study of the combined effects of the air-gap transfer for Maxwell tensor and the tooth mechanical modulation in electrical machines," *IEEE Trans. Magn.*, vol. 56, no. 1, Jan. 2020, Art. no. 7502004.

[11] Y. Zhou, J. Ji, W. Zhao, S. Zhu, and H. Liu, "Modulated vibration reduction design for integral-slot interior permanent magnet synchronous machines," *IEEE Trans. Ind. Electron.*, vol. 69, no. 12, pp. 12249–12260, Dec. 2022.

[12] J. Hong, S. Wang, Y. Sun, and H. Cao, "A high-precision analytical method for vibration calculation of slotted motor based on tooth modeling," *IEEE Trans. Ind. Appl.*, vol. 57, no. 4, pp. 3678–3686, Jul./Aug. 2021.
[13] H. Yin, H. Zhang, W. Hua, Z. Wu, and C. Li, "Quantitative analysis of electromagnetic forces by decoupling air-gap field modulation and force modulation in rotor-permanent-magnet machines," *IEEE Trans. Ind. Electron.*, vol. 70, no. 2, pp. 1310–1320, Feb. 2023.
[14] S. Wang, J. Hong, Y. Sun, and H. Cao, "Analysis of zeroth-mode slot frequency vibration of integer slot permanent-magnet synchronous motors," *IEEE Trans. Ind. Electron.*, vol. 67, no. 4, pp. 2954–2964, Apr. 2020.
[15] S. Zhu, W. Zhao, J. Ji, G. Liu, Y. Mao, and T. Liu, "Investigation of bread-loaf magnet on vibration performance in FSCW PMSM considering force modulation effect," *IEEE Trans. Transp. Electrific.*, vol. 7, no. 3, pp. 1379–1389, Sep. 2021.
[16] W. Liang, J. Wang, P. C.-K. Luk, and W. Fei, "Analytical study of stator tooth modulation on electromagnetic radial force in permanent magnet synchronous machines," *IEEE Trans. Ind. Electron.*, vol. 68, no. 12, pp. 11731–11739, Dec. 2021.
[17] Y. Mao, W. Zhao, S. Zhu, Q. Chen, and J. Ji, "Vibration investigation of spoke-type PM machine with asymmetric rotor considering modulation effect of stator teeth," *IEEE Trans. Ind. Electron.*, vol. 68, no. 10, pp. 9092–9103, Oct. 2021.
[18] W. Zhao, S. Zhu, J. Ji, G. Liu, and Y. Mao, "Analysis and reduction of electromagnetic vibration in fractional-slot concentrated-windings PM machines," *IEEE Trans. Ind. Electron.*, vol. 69, no. 4, pp. 3357–3367, Apr. 2022.
[19] H. Fang, D. Li, J. Guo, Y. Xu, and R. Qu, "Hybrid model for electromagnetic vibration synthesis of electrical machines considering tooth modulation and tangential effects," *IEEE Trans. Ind. Electron.*, vol. 68, no. 8, pp. 7284–7293, Aug. 2021.
[20] J.-H. Kim, S.-H. Park, J.-Y. Ryu, and M.-S. Lim, "Comparative study of vibration on 10-pole 12-slot and 14-pole 12-slot PMSM considering tooth modulation effect," *IEEE Trans. Ind. Electron.*, vol. 70, no. 4, pp. 4007–4017, Apr. 2023.
[21] S. Wang, J. Hong, Y. Sun, and H. Cao, "Mechanical and magnetic pivot roles of tooth in vibration of electrical machines," *IEEE Trans. Energy Convers.*, vol. 36, no. 1, pp. 139–148, Mar. 2021.
[22] S. Zhu, W. Zhao, J. Ji, G. Liu, and C. H. T. Lee, "Design to reduce modulated vibration in fractional-slot concentrated-windings PM machines considering slot-pole combination," *IEEE Trans. Transp. Electrific.*, vol. 9, no. 1, pp. 575–585, Mar. 2023.
[23] R. A. Toupin, "Saint-Venant's principle," *Arch. Ration. Mech. Anal.*, vol. 18, no. 2, pp. 83–96, 1965.
[24] R. C. Hibbeler, *Mechanics of Materials*, 5th ed. Upper Saddle River, NJ, USA: Pearson Educ., 2003.

Jae-Hyun Kim received the bachelor's degree in mechanical engineering and the Ph.D. degree in automotive engineering from Hanyang University, Seoul, South Korea, in 2017 and 2023, respectively. Since 2023, he has been with R&D Division of Hyundai Mobis, Uiwang, South Korea. His research interests include the design, and the analysis of vibration and noise of electric machines.

Jun-Yeol Ryu received the bachelor's degree in mechanical engineering and electronic systems engineering from Hanyang University, Ansan, South Korea, in 2016, and the Ph.D. degree in automotive engineering with Hanyang University, Seoul, South Korea, in 2023. Since 2023, he has been with Korea Automotive Technology Institute, Cheonan, South Korea, where he is currently a Senior Researcher. His research interests include design and optimization of electric machines and analysis of electro-magnetic field.

Soo-Hwan Park received the bachelor's degree in mechanical engineering and the Ph.D. degree in automotive engineering from Hanyang University, Seoul, South Korea, in 2014 and 2022, respectively. From 2019 to 2020, he was with the Korea Institute of Industrial Technology, Daegu, South Korea. From 2022 to 2023, he was with R&D Division of Hyundai Motor Company, Hwaseong, South Korea. Since 2023, he has been with the Department of Mechanical, Robotics, and Energy Engineering, Dongguk University, Seoul, South Korea, as an Assistant Professor. His research interests include electromagnetic field analysis, design and optimization of electric machines for automotive and robotics applications, and thermal management system for electric-driven mobility system.

Kyoung-Soo Cha received the bachelor's degree in electric engineering from Chungbuk University, Cheongju, South Korea, in 2015, and the Ph.D. degree in automotive engineering from Hanyang University, Seoul, South Korea, in 2022. In 2022, he was a Postdoctoral Researcher with Hanyang University, Seoul, South Korea. Since 2022, he has been with the Korea Institute of Industrial Technology, Daegu, South Korea, where he is currently Postdoctoral Reseacher. His research interests include electric machine design for automotive and home appliance, system modeling and optimization of electric vehicles, hybrid electric vehicle, and fuel cell electric vehicles.

Yun-Jae Won (Graduate Student Member, IEEE) received the bachelor's degree in automotive engineering in 2021 from Hanyang University, Seoul, South Korea, where he is currently working toward the Ph.D. degree in automotive engineering. His research interests include the design, and vibration and noise of electric machines.

Chi-Sung Park received the master's degree in electrical engineering from Pusan National University, Pusan, South Korea, in 2011. He is currently working the Ph.D. degree in automotive engineering from Hanyang University, Seoul, South Korea. Since 2010, he has been with LG Electronics, Changwon, South Korea, where he is currently a Senior Research Engineer. His research interests include the design, and the analysis of vibration and noise of electric machines.

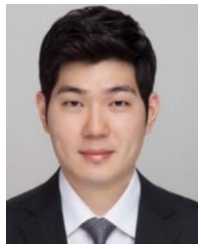

Myung-Seop Lim (Senior Member, IEEE) received the bachelor's degree in mechanical engineering and the master's and Ph.D. degrees in automotive engineering from Hanyang University, Seoul, South Korea, in 2012, 2014, and 2017, respectively.

From 2017 to 2018, he was a Research Engineer with Hyundai Mobis, Yongin, South Korea. From 2018 to 2019, he was an Assistance Professor with Yeungnam University, Daegu, South Korea. Since 2019, he has been with Hanyang University, Seoul, South Korea, where he is currently an Assistant Professor.

His research interests include electromagnetic field analysis and multi-physics analysis of electric machinery for mechatronics systems, such as automotive and robot applications.